

Fluorescence intensity in surface-plasmon field-enhanced fluorescence spectroscopy

S. Ekgasit^{a,b,*}, F. Yu^b, W. Knoll^b

^a Sensor Research Unit, Department of Chemistry, Faculty of Science, Chulalongkorn University, Bangkok 10330, Thailand

^b Max-Planck-Institut für Polymerforschung, Ackermannweg 10, D-55128 Mainz, Germany

Received 7 February 2004; received in revised form 20 May 2004; accepted 24 May 2004

Available online 20 July 2004

Abstract

Reflection loss in surface-plasmon resonance (SPR) curve of an absorbing dielectric is due to the absorptions of the metal film and the absorbing dielectrics. The SPR curve is significantly distorted from that of the nonabsorbing dielectric (i.e., broader curve shape with higher reflectance minimum), especially for strong absorbing dielectrics. When absorption of the absorbing dielectric is too small (i.e., very thin or low concentration), insignificant change in SPR curve is observed as the absorbing dielectric binds onto a nonabsorbing dielectric film. However, if the absorbing dielectrics are fluorophores or fluorophore-labeled molecules, the presence of small amount of the absorbing dielectric can be detected by the highly sensitive surface-plasmon field-enhanced fluorescence spectroscopy (SPFS). The fluorescence signal can be expressed in terms of the dielectric constant of the absorbing dielectric and the SPR-generated evanescent field. Although the fluorescence quenching near the metal surface complicates the SPFS-fluorescence signal, the quantitative analysis can be performed on a well-defined dielectric layer.

© 2004 Elsevier B.V. All rights reserved.

Keywords: Surface-plasmon resonance; SPR; SPFS; Fluorescence; Evanescent field

1. Introduction

Surface-plasmon resonance (SPR) spectroscopy takes advantage of the strong SPR-generated evanescent field at the surface of a thin noble metal film for probing thin dielectric films deposited on the metal surface. The exponential decay characteristic of the SPR-generated evanescent field makes SPR sensor very sensitive to chemical or physical interactions that can induce thickness and/or complex refractive index variations near the metal surface [1,2]. As the refractive index and/or the thickness of the dielectric film change, the resonance angle shifts to a new position. The magnitude of the angle shift and/or the variation of the reflectance at a certain angle of incidence can be correlated to the physicochemical phenomena at the interface. The kinetics of the reactions, binding events as well as properties of the dielectric film under various environments and experimental conditions can be followed [2–6].

Since an observable change in the SPR curve is induced by thickness and/or refractive index changes, binding events

associate with molecules and/or small number of molecules such as protein fragment and small drug molecules cannot be detected by SPR technique due to insignificant change at the surface [7–9]. In order to improve sensitivity of the SPR-based sensing technique, the surface sensitive SPR phenomenon is combined with fluorescence spectroscopy. By coupling the strong SPR-generated evanescent field to a layer of fluorophores or fluorophore-labeled molecules confined near the metal surface, the fluorescence signal can be pickup by a sensitive detector. The highly surface sensitive nature of surface-plasmon field-enhanced fluorescence spectroscopy (SPFS) has proven to be a complementary to SPR technique where additional chemical information together with physical information of the thin film at the interface can be collected simultaneously [7–9]. The combination of the highly sensitive nature of the fluorescence technique with the strong SPR-generated evanescent field makes SPFS exceptionally sensitive to minute changes associated with fluorophores. A detection limit less than 240 pM of human chorionic gonadotrophin (hCG) was observed via SPR-based fluoroimmunoassay [10]. A multicomponent macromolecular adsorption onto the surface of functionalized self-assembled monolayer from an aqueous solution was reported [11]. Binding events between antibody-bound

* Corresponding author. Tel.: +66-2-218-7585;
fax: +66-2-218-7598/254-1309.
E-mail address: sanong.e@chula.ac.th (S. Ekgasit).

self-assembled monolayer and its antigen were studied by the SPR–SPFS technique [12].

Although SPFS is a very sensitive SPR-based sensing technique, the quantitative analysis of the fluorescence signal is complicated by the fluorescence quenching via a non-radiative resonance energy transfer near the metal surface [13–18]. The distance-dependent resonance energy transfer quenches all the emitted fluorescence if the fluorophores are too close to the metal film. In order to perform a quantitative analysis of the SPFS-fluorescence signal, an insight on the distance-dependent amplitude of the SPR-generated evanescent field is required. This paper will show the linear relationship between the SPFS-fluorescence intensity and the SPR-generated evanescent field. A quantitative analysis of the SPFS-fluorescence signal of a well-defined absorbing dielectric film will be examined.

2. Theory and simulations

For an SPR setup in the Kretschmann–Raether ATR configuration, reflectance of a multilayer (i.e., metal film/dielectric films/dielectric substrate) depends strongly on the experimental conditions (i.e., angle of incidence and wavelength of the coupled radiation) and material characteristics (i.e., complex refractive indices of metal film, dielectric films and dielectric substrate, and thickness of metal and dielectric films). Under ATR condition, the reflectance $R(\theta)$ of the coupled radiation with parallel polarization can be expressed in terms of the evanescent field amplitude by [19–21]:

$$R(\theta) = 1 - A(\theta)$$

$$= 1 - \left(\frac{2\pi}{\lambda} \right)^2 \frac{1}{k_{zP}(\theta)} \sum_{j=1}^N \left[\int_{z_j}^{z_{j+1}} \text{Im}[\hat{\epsilon}_j] \langle E_z^2(\theta) \rangle dz \right] \quad (1)$$

where θ is the angle of incidence, $A(\theta)$ the absorption in *absorbance* unit, λ the wavelength of the couple radiation, $\hat{\epsilon}_j$ the complex dielectric constant of the j th layer, and $\langle E_z^2(\theta) \rangle$ the mean square evanescent electric field (MSEF) at a distance z from the metal/prism interface. N is the number of film in the multilayer with the metal film as the first layer. $k_{zP}(\theta)$ is the z -component of the wavevector in the prism. $k_{zP}(\theta)$ can be expressed in terms of the x -component of the wavevector $k_{xP}(\theta)$ by $k_{zP}(\theta) = [(2\pi/\lambda)^2 \epsilon_P - k_{xP}^2(\theta)]^{1/2}$ with $k_{xP}(\theta) = (2\pi/\lambda)[\epsilon_P \sin^2 \theta]^{1/2}$ and ϵ_P is the dielectric constant of the prism. The detailed derivations of the SPR-reflectance associated with MSEF are given elsewhere [20–22].

2.1. SPR of nonabsorbing dielectrics

In the conventional SPR, change associated with nonabsorbing dielectric film are of interest. SPR of a system where

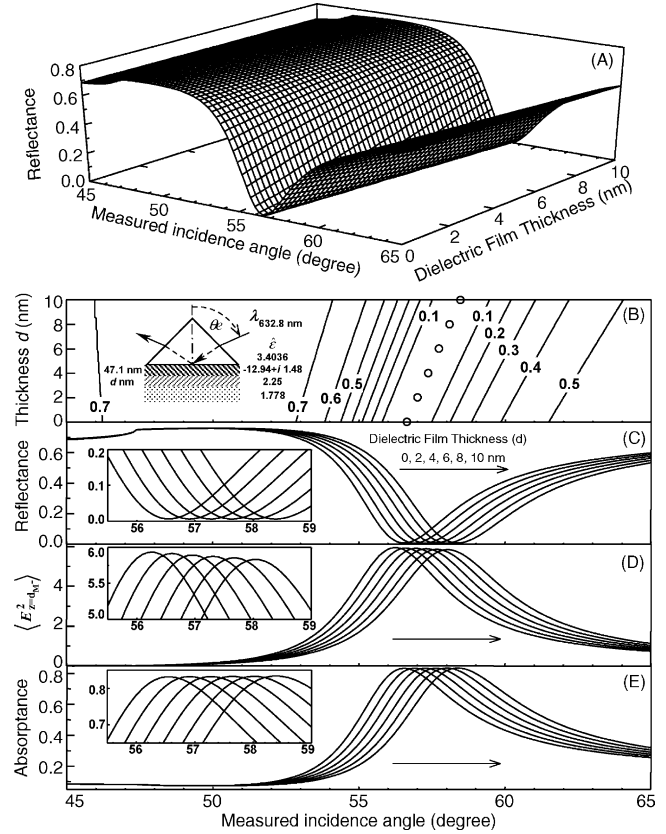


Fig. 1. (A) 3D-surface plot; (B) the corresponding contour plot of angle-scan SPR curves of a four-phase system as the dielectric film thickness increases; (C) SPR curves at selected thickness of the dielectric film; (D) MSEFs at the metal/dielectric interface (on the metal side); and (E) absorption of the metal film. The simulation parameters are: $\epsilon_P = 3.4036$, $\hat{\epsilon}_{Au} = -12.94 + i1.48$, $d_{Au} = 47.1$ nm, $\hat{\epsilon}_{DF} = 2.25$, $\epsilon_{DS} = 1.778$. The arrows indicate the direction of changes as thickness increases.

binding events build up a thicker dielectric layer on top of the metal film can be simply modeled by a four-phase Fresnel equation. SPR curves of a four-phase system (prism/gold film/nonabsorbing dielectric film/nonabsorbing dielectric substrate) are shown in Fig. 1. Since the gold film is the only absorbing medium, the SPR reflectance of the system can be expressed in terms of the absorption of the gold film as

$$R(\theta) = 1 - \left(\frac{2\pi}{\lambda} \right)^2 \frac{1}{k_{zP}(\theta)} \int_0^{d_{Au}} \text{Im}[\hat{\epsilon}_{Au}] \langle E_z^2(\theta) \rangle dz \quad (2)$$

where d_{Au} and $\hat{\epsilon}_{Au}$, respectively, are thickness and complex dielectric constant of the gold film. The resonance angle shifts to a greater value as the thickness of the film increases. The magnitude of the shift increases linearly with the thickness of the nonabsorbing dielectric film. According to SPR curves at selected film thickness, Fig. 1C, the reflectance minimum at the resonance angle insignificantly changes as the thickness increases. This phenomenon associates with the MSEF at the metal/dielectric interface. Although the MSEF amplitude at the metal/dielectric interface slightly decreases as the dielectric film thickness increases, Fig. 1D, absorption of the gold film insignificantly changes, Fig. 1E,

due to the angle-dependent nature of the wavevector $k_{zP}(\theta)$ [21]. The slightly decreased $k_{zP}(\theta)$ compensates for the small decrease of the MSEF at the interface as the angle of incidence increases.

Although the reflectance is directly derived from the MSEF, the resonance angle is slightly greater than the angle with field maximum of the corresponding MSEF at the metal/dielectric interface, Fig. 1C and D. This phenomenon associates with the decay characteristics of the MSEF within the metal film. The MSEF decays exponentially while the field maximum shifts toward a greater angle as the distance from the interface increases [21]. The MSEF integration within the metal film, as a result, has a maximum at the resonance angle.

Fig. 1 suggests that the variation of the nonabsorbing dielectric film thickness does not induce any significant change of the reflectance minimum but does alter the surface-plasmon resonance condition, which result in a linear shift of the resonance angle. This unique phenomenon enables SPR sensor quantitatively analyzes binding events of nonabsorbing dielectrics.

2.2. SPR of absorbing dielectrics

SPR curve of an absorbing dielectric is characterized by a broader curve shape together with a greater reflectance minimum due to the presence of an additional absorbing dielectric, as shown in Fig. 2. The reflectance of a simple four-phase system (prism/metal film/absorbing dielectric film/nonabsorbing dielectric substrate) can be expressed in terms of the absorptions of the metal and the absorbing dielectric films as

$$R(\theta) = 1 - \left(\frac{2\pi}{\lambda}\right)^2 \frac{1}{k_{zP}(\theta)} \left\{ \int_0^{d_{Au}} \text{Im}[\hat{\epsilon}_{Au}] \langle E_z^2(\theta) \rangle dz + \int_{d_{Au}}^{d_{Au}+d_{AD}} \text{Im}[\hat{\epsilon}_{AD}] \langle E_z^2(\theta) \rangle dz \right\} \quad (3)$$

where d_{AD} and $\hat{\epsilon}_{AD}$, respectively, are thickness and complex dielectric constant of the absorbing dielectric film. As thickness of the absorbing dielectric increase, the resonance angle linearly shifts to a greater value, the SPR curves become broader while the reflectance minimum becomes greater. It should be noted that resonance angle of the absorbing dielectric is slightly greater than that of the nonabsorbing dielectric of the same layer architecture. Due to the influence of the absorbing dielectric, the evanescent field at the metal/dielectric interface is less enhanced compared to that of the nonabsorbing dielectric. The total absorption of the system (i.e., absorptions of the gold film and the absorbing dielectric film) is smaller compared to that of the nonabsorbing dielectric. The phenomenon can be visualized by a greater reflectance minimum and a broader peak shape as the absorption of the absorbing dielectric increases (i.e., via the incre-

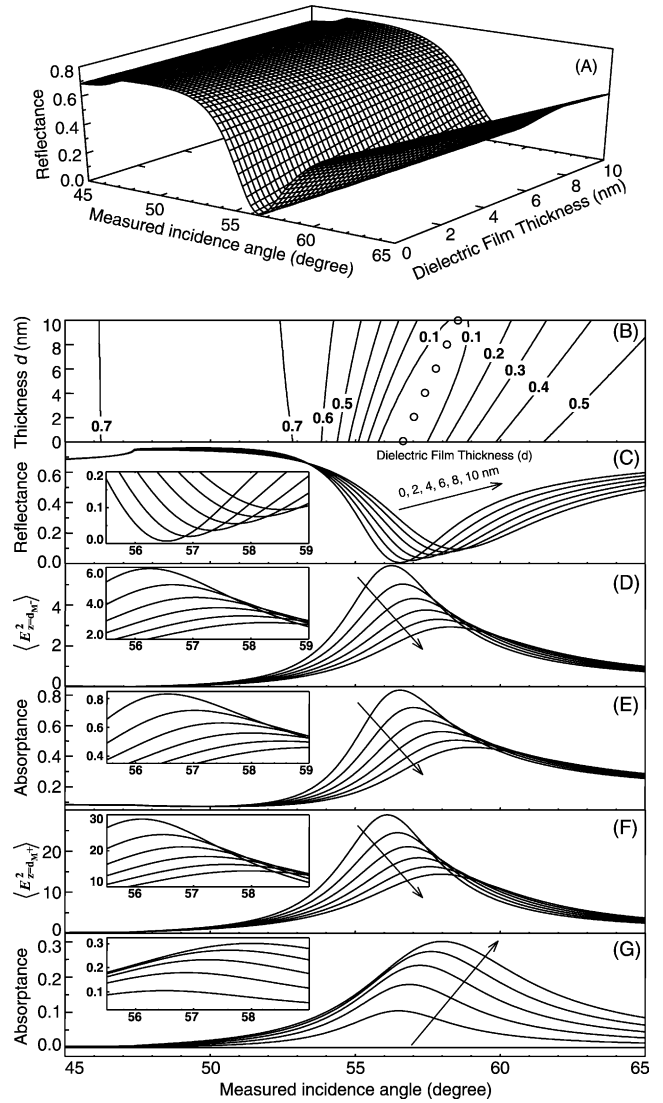


Fig. 2. (A) 3D-surface plot; (B) the corresponding contour plot of angle-scan SPR curves of a four-phase system as the dielectric film thickness increases; (C) SPR curves at selected thickness of the dielectric film; (D) MSEFs at the metal/dielectric interface (on the metal side); (E) absorption of the metal film; (F) MSEFs at the metal/dielectric interface (on the dielectric side); and (G) absorption of the absorbing dielectric film. The simulation parameters are the same as those in Fig. 1 with $\hat{\epsilon}_{DF} = 2.25 + i0.3$. The arrows indicate the direction of changes as thickness increases.

ments of thickness and/or imaginary part of the dielectric constant).

The optical enhancement at the metal/dielectric interface makes the MSEF on the dielectric side much greater than that on the metal side while the wavevector-dependent nature of the MSEF makes the angle with field maximum on the dielectric side smaller than that on the metal side, see Fig. 2D and F. Similar to that of the nonabsorbing dielectric film, the resonance angle is slightly greater than the corresponding angle with field maximum of the MSEF at the metal/dielectric interface. The MSEF decay characteristic within the metal film makes the angle with absorption maxi-

imum of the metal film greater than the angle with field maximum at the interface (on the metal side), Fig. 2D and E. On the dielectric side, since the angle with field maximum does not change as the MSEF decays into the dielectric media, the angle with absorption maximum of the dielectric film is the same as the angle with field maximum at the metal/dielectric interface (on the dielectric side), Fig. 2F and G. According to Eq. (3), the resonance angle is between the angle with maximum dielectric absorption and the angle with maximum metal absorption, as shown in Fig. 2C, E and G. Beside the decrease of the MSEF at the interface, the difference of the angles with absorption maximums also contributes to the broad feature of the SPR curve of an absorbing dielectric.

Due to exponentially decay characteristic of the evanescent field and the decrease of the evanescent field enhancement at the interface, absorptance of the absorbing dielectric film does not increase in a linear fashion with the film thickness. Although the resonance angle of the absorbing film increase linearly with the thickness of the absorbing dielectric, the resonance angle becomes less obvious as the absorption of the dielectric film increases.

2.3. Fluorescence intensity in SPR–SPFS

SPR–SPFS takes advantages of the strong SPR-generated evanescent field at the metal/dielectric interface to excite the confined fluorophores near the interface. Since SPFS-fluorescence intensity corresponding to SPR-reflectance can be observed, chemical information from SPFS curve together with physical information from SPR curve can be obtained simultaneously. Due to a linear relationship between absorption and fluorescence emission [23,24], the SPFS-fluorescence intensity $I_{\text{Fluorescence}}$ can be expressed in terms of the MSEF by the following expression [21]:

$$I_{\text{Fluorescence}}(\theta) = K_{\text{Optics}} \left(\frac{2\pi}{\lambda} \right)^2 \frac{1}{k_{\text{zP}}(\theta)} \times \int_{d_{\text{Fluorophore}}} K_{\text{RET}}(z) \text{Im}[\hat{\epsilon}_{\text{Fluorophore}}] \langle E_z^2(\theta) \rangle dz \quad (4)$$

where $\hat{\epsilon}_{\text{Fluorophore}}$ is the dielectric constant of the dielectric film with fluorophores, $K_{\text{RET}}(z)$ is the fluorescence quenching factor due to the resonance energy transfer. $\int_{d_{\text{Fluorophore}}}$ indicates an integration over the thickness of the layer with fluorophores. K_{Optics} is a constant whose value depends on experimental parameters (i.e., attenuation factor, filter, focusing lens, and optical windows).

3. Experimental

3.1. Setup for SPR–SPFS measurement

A schematic illustration of an SPR–SPFS setup is shown in Fig. 3. For SPR measurement, a radiation from a HeNe laser ($\lambda = 632.8 \text{ nm}$, 10 mW, Uniphase, USA) is modulated

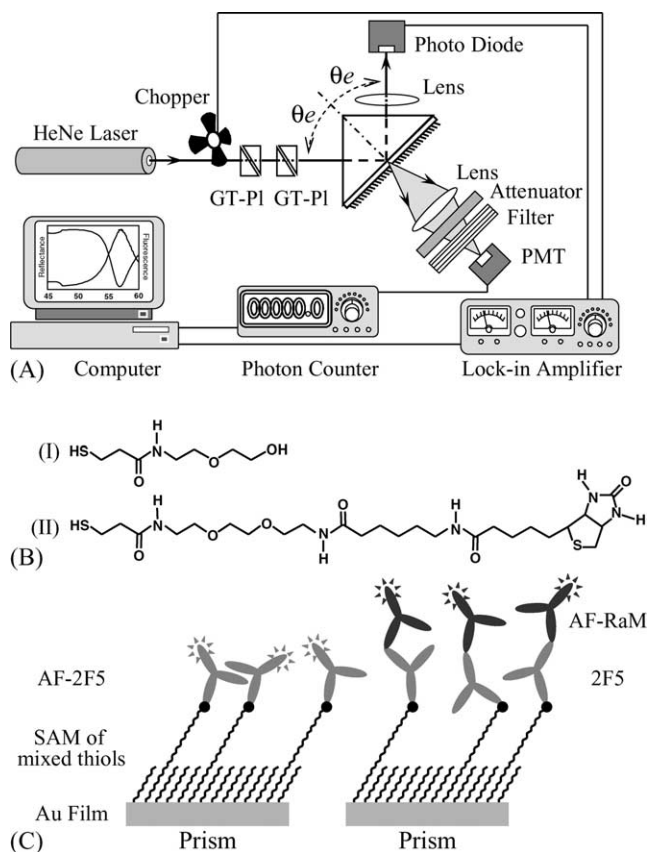


Fig. 3. (A) A schematic illustration of the SPR–SPFS setup. (B) Structures of thiols employed for mixed SAM fabrication: (I) OH-terminated thiol and (II) biotin-terminated thiol. (C) Schematic drawings of the antibody-bound SAM employed for the SPR–SPFS experiments. Note: AF-2F5 and AF-RaM are fluorophore-labeled antibodies.

by a chopper. The plane of polarization and intensity of the modulated radiation are controlled by two Glan-Thompson polarizers (GT-PI). The radiation is coupled to the multilayer via a right-angled prism (LASFN9, $\epsilon = 3.4036$, Schott Glas, Germany). The reflected beam is focused onto a photodiode detector by a lens ($f = 50 \text{ mm}$, Owis, Germany). The corresponding SPFS signal is collected from the backside of the prism by focusing the fluorescence light with a lens ($f = 50 \text{ mm}$, Owis, Germany), passing through a neutral filter and an interference filter ($\lambda = 670 \text{ nm}$, $\Delta\lambda = 10 \text{ nm}$, LOT, 80% transmission), onto a photomultiplier tube (PMT, Hamamatsu, Japan). The PMT is connected to a photon counter unit (Agilent, USA) where the fluorescence signal is expressed as photon counts per second, cps. The neutral filter, which functions as an attenuator, keeps the signal from PMP within its linear range (i.e., less than 1×10^6 cps). The current experiments employ attenuation factor of 60.88. The factor is obtained from an independent calibration measurement.

The SPR signal is collected as a function of the angle θ_e defined with respect to the direction normal to the prism/metal interface. A homemade program controls a precise angular rotation of the goniometer where the prism and

flow cell are mounted. The measured incidence angle θ_e from the goniometer is slightly different from the actual angle of incidence θ at the prism/metal interface due to the difference between refractive index of air and refractive index of prism. The relationship between the two angles is given by $\theta_e = \sin^{-1}[\epsilon_p^{1/2} \sin(\theta - \varphi)] + \varphi$, where $\varphi = 45^\circ$ for a right-angled prism. For direct comparisons with the experimental results, the simulated results are expressed as functions of the measured angle of incidence. The simulated results are corrected for the reflection at the air/prism interface.

3.2. Preparation of self-assembled monolayer of mixed thiol (SAM)

LASFN9 slides were cleaned and coated with ~ 50 nm gold film via a commercially available thermal evaporation instrument (Edwards, England). A solution of mixed thiols, OH-terminated thiol and biotin-terminated thiol, with a net thiol concentration of $500 \mu\text{M}$ at a mole fraction of the biotin-terminated thiol of 0.004, was prepared in absolute ethanol. The self-assembled monolayer of mixed thiols was fabricated by immersing the gold-coated LASFN9 slides in the solution over night at room temperature. The substrates were rinsed thoroughly with absolute ethanol, blown-dry with dry nitrogen, and kept under argon environment until being used.

3.3. Materials and experimental procedures

The anti-biotin mouse monoclonal antibody 2F5 (isotype IgG_{1,k}), the Alexa Fluor 647-labeled rabbit anti-mouse IgG (dye-to-protein ratio = 4.8), and the Alexa Fluor 647 monoclonal antibody labeling kit were purchased from Molecular Probes. The 2F5 antibody was labeled with Alexa Fluor 647 dye by following a standard protocol provided by Molecular Probes. The dye-to-protein ratio was 4.4 as determined by a spectroscopic approach. Sodium dodecyl sulfate (SDS) and phosphate-buffered saline (PBS) tablets were purchased from Sigma-Aldrich. An HBS-EP buffer (degassed 10 mM HEPES-buffered saline, pH 7.4, 150 mM NaCl, 3 mM EDTA with 0.005% (v/v) surfactant P-20, Biacore, Sweden) was employed for the preparation of the protein solutions.

For simplicity, the fluorophore-labeled rabbit anti-mouse IgG is represented by AF-RaM while the fluorophore-labeled anti-biotin mouse monoclonal antibody 2F5 is represented by AF-2F5.

All experiments were performed at room temperature ($21 \pm 2^\circ\text{C}$) with HBS-EP as a buffer solution. An aliquot of 1 mL sample solution was injected into the flow cell. The sample is left in the flow cell for 15 min to allow a complete binding on the surface of SAM. The cell was then flow-washed and filled with running buffer to avoid bulk solution effects. The working concentration of 2F5, AF-2F5, and AF-RaM are 20, 20, and 33 nM, respectively.

The antibody-bound SAM can be regenerated by an SDS solution (5 mg/mL in HBS-EP). Once the generation is completed, further binding events can be performed. Schematic illustrations of layer architectures of the antibody-bound SAM are shown in Fig. 3 [12,25].

4. Results

Fig. 4 shows angle-scan SPR curves and corresponding SPFS curves of antibody-bound SAM. As the antibodies bind onto the surface of SAM, the resonance angle and the fluorescence angle $\theta_{\text{Fluorescence}}$ (i.e., the angle with the maximum fluorescence intensity) shift to a greater value. The fluorescence angle is always smaller than the corresponding resonance angle. In order to determine the dielectric constant and the thickness of each dielectric layer (i.e., SAM, AF-2F5, 2F5, and AF-RaM) the SPR curves are fitted with reflectance calculated by Fresnel equation. Comparisons between observed and calculated SPR curves are shown in Fig. 5.

As the fluorophore-labeled AF-2F5 is bound onto SAM, the resonance angle shifts to a greater value, the reflectance minimum slightly increases and SPR curve is slightly broaden, Fig. 4A(a) and A(b). The corresponding SPFS curves indicate no fluorescence emission from SAM but strong fluorescence of 5400 cps from AF-2F5 bound SAM, Fig. 4B(a) and B(b). When AF-2F5 is removed, the resonance angle retreat back to the same value as that of the virgin SAM, Fig. 4A(c). The SPR curve of the virgin regenerated SAM and that of the generated SAM cannot be differentiated graphically. The corresponding SPFS curve of the regenerated SAM, Fig. 4B(c), however, shows fluorescence signal of 200 cps. When a non-labeled antibody 2F5 is bound onto the surface of SAM, the resonance angle shifts to a greater value while reflectance minimum

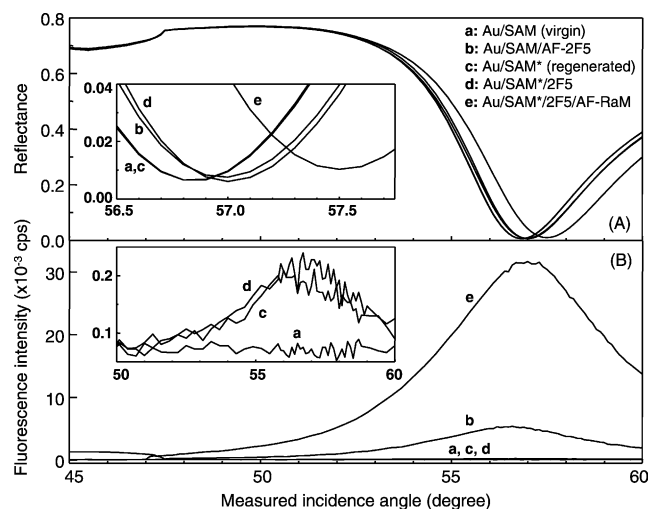


Fig. 4. (A) Experimentally measured SPR curves of the antibody-bound SAM and (B) their corresponding SPFS curves.

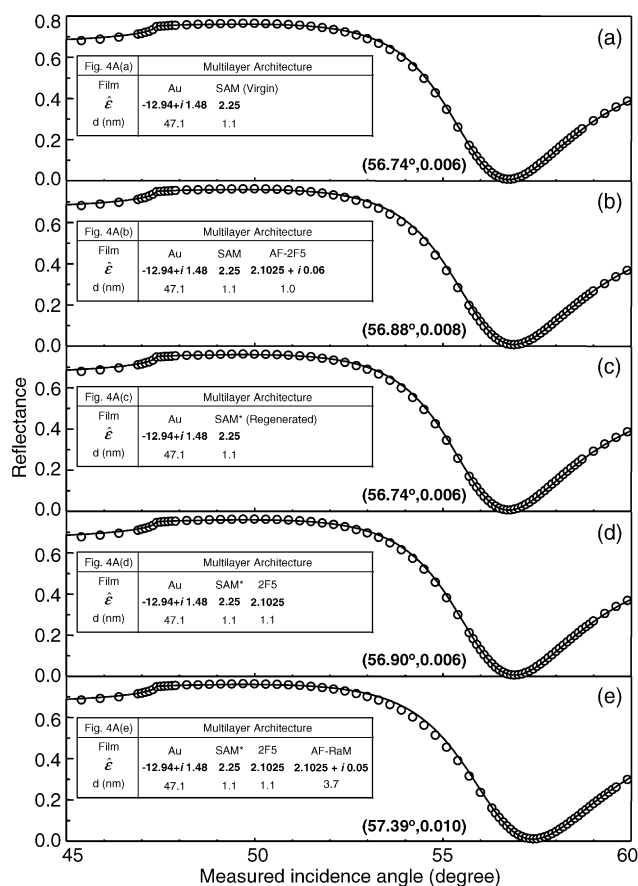


Fig. 5. Comparison between experimentally measured SPR curves (open circles) and the corresponding best-fit curves calculated by Fresnel equation. The best-fit parameters are shown in insets: dielectric constant of prism $\epsilon_p = 3.4036$ and dielectric constant of HBS-EP $\epsilon_{\text{HBS-EP}} = 1.778$. The numbers in parenthesis indicate resonance angle and reflectance minimum. The figure labels are associated with layer architecture defined in Fig. 4. Note: the calculated SPR curves are corrected for reflections at the air/prism and prism/air interfaces.

stays unchanged, Fig. 4A(d). Interestingly, the corresponding SPFS curve shows an increased fluorescence signal, 230 cps, Fig. 4B(d). When the fluorophore-labeled AF-RaM is subsequently bound onto the 2F5-bound SAM, the resonance angle shifts to a greater value, the reflectance minimum slightly increases and SPR curve is slightly broaden, Fig. 4A(e). A maximum fluorescence signal of 31 500 cps is observed, Fig. 4B(e).

5. Discussion

The indifference between SPR curves of the virgin SAM and the regenerated SAM, Fig. 4A(a) and A(c), indicates the same refractive index and thickness of the dielectric films. However, the corresponding SPFS curve of the regenerated SAM indicates a residual AF-2F5 on the surface of the regenerated SAM. Although the absorption of the residual AF-2F5 is too small to induce a significant reflectance

change in the observed SPR curve, the SPR-enhanced absorption of the fluorophores can be detected via the emitted fluorescence of the excited fluorophores. This observation implies the highly sensitive nature of SPFS technique. It is so sensitive that it can detect a small number of bound molecules where the thickness increment is too small to induce a significant change in the corresponding SPR curve.

A small increment of the fluorescence signal when the 2F5 was bound onto the regenerated SAM indicates that the residual AF-2F5 molecules move away from surface the metal film where the fluorescence quenching decreases, Fig. 4B(c) and B(d). The displacement is imposed by the neighboring 2F5 molecules. Due to flexibility of the long chain biotin-terminated thiols, the residual AF-2F5 molecules lie close to SAM surface before the binding of 2F5. Since the number of biotin-terminated thiols is small compared to that of the OH-terminated thiols, the number of bound 2F5 on the surface of SAM is still too low, thus, the separation of residual AF-2F5 from the metal film was not substantially increased. The same reflectance minimums of the corresponding SPR curves, Fig. 4A(c) and A(d), implies that the MSEFs at the metal/dielectric interfaces are the same, thus, the MSEF decay profiles in the metal film of both systems are exactly the same. Due to the difference in the layer architectures, the residual AF-2F5 on the regenerated SAM, Fig. 6c, experiences a stronger MSEF compared to that in the 2F5-bound regenerated SAM, Fig. 6d. However, the latter emits even stronger fluorescence signal than the former. Thus, the small increment of the fluorescence signal is due solely to the decrease of fluorescence quenching efficiency by a slightly larger separation of the residual AF-2F5 from the metal surface after the subsequent binding of 2F5.

The influence of fluorescence quenching is obvious in SPFS curves of AF-2F5 and AF-RaM, Fig. 4B(b) and 4B(e). Their corresponding SPR curves have about the same magnitudes of reflectance minimums. This implies that the corresponding absorptions of the fluorophore-labeled

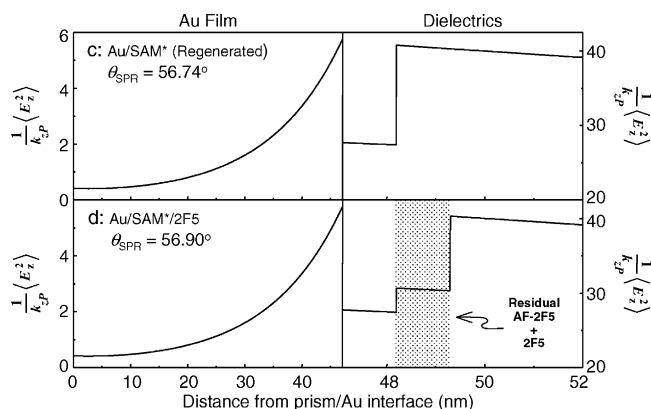


Fig. 6. MSEF decay profile in (c) regenerated SAM and (d) 2F5-bound SAM at the resonance angle. The residual AF-2F5 molecules are confined near SAM surface. The parameters for the MSEF calculations are the best-fit parameters of SPR curves shown in Fig. 5. The figure labels are associated with layer architecture defined in Fig. 4.

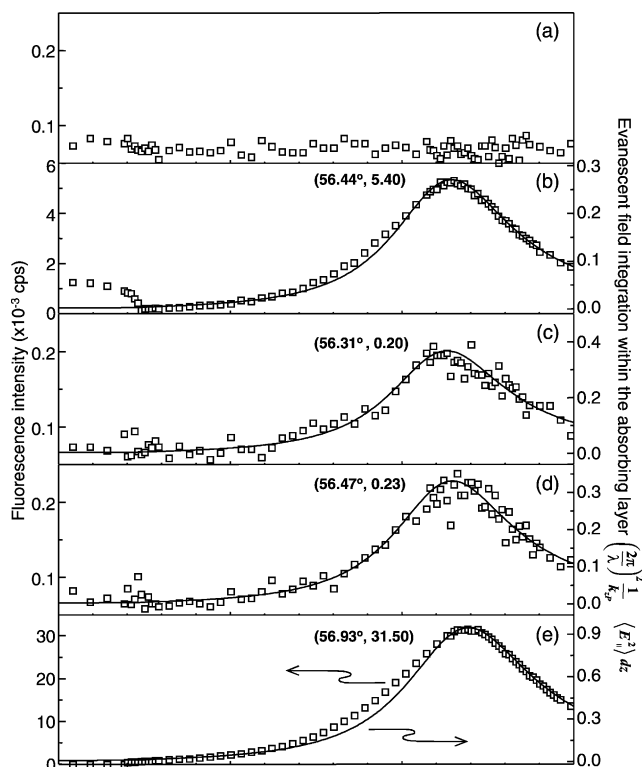


Fig. 7. Comparisons between the experimentally measured fluorescence intensities (open squares) and the corresponding MSEF integrations within the layers with fluorophore labeling (solid lines). The parameters for the MSEF calculations are the best-fit parameters of SPR curves shown in Fig. 5. The numbers indicate fluorescence angles and the corresponding fluorescence signals. The figure labels are associated with layer architecture defined in Fig. 4.

antibodies are about the same. However, the fluorescence intensity of AF-RaM is much greater than that of the AF-2F5. Due to a greater separation of AF-RaM from the metal film compared to that of the AF-2F5, a weaker resonance energy transfer quenches less fluorescence intensity of the excited fluorophore in the AF-RaM. As a result, a 5.8 times stronger fluorescence intensity is observed from AF-RaM compared to that of AF-2F5.

Since the fluorescence intensity has a linear relationship with the absorption of the excited molecules, fluorescence signal from SPFS can be linearly expressed in terms of the MSEF integration within the absorbing layer. Comparisons between the observed fluorescence signals and the corresponding MSEF integrations within the absorbing layer are shown in Fig. 7. Excellent agreements between the fluorescence signals and the MSEF integrations are observed. The observed fluorescence angles are accurately predicted by the angles with maximum absorptions, which are the same as the angle with field maximum at the metal/dielectric interface (on the dielectric side).

Due to complications by the distance-dependent fluorescence quenching, a quantitative analysis of SPFS-fluorescence signals cannot be performed. However, with carefully controlled layer architectures of the multilayer (i.e., the lay-

ers with fluorophores are at the same distance from the metal film), a quantitative analysis of the fluorescence signal can be carried out. According to observed SPR curves and the fitting parameters, films of AF-2F5 and 2F5 (with residual AF-2F5 molecules), Fig. 4A(b) and 4A(d), respectively, have approximately the same thickness (i.e., 1.0 nm versus 1.1 nm at $\epsilon = 2.1025$) while being separated from the metal film at the same distance. This implies that the fluorophores in both films are subjected to approximately the same quenching efficiency. Due to the small fraction of biotin-terminated thiol together with small degree of self-quenching by neighboring dye molecules in Alexa Fluoro 647 dye at high concentration [26,27], no self-quenching in the fluorophore-labeled AF-2F5 layer is assumed. According to the above assumption, the regeneration of antibody-bound SAM by SDS eliminated 97% of the originally bound antibodies, as calculated from the observed SPFS-fluorescence signals at the fluorescence angles with background noise correction (70 cps, Fig. 7a).

6. Conclusions

For SPR of a nonabsorbing dielectric film, the resonance angle linearly shifts to a greater value as the thickness of the dielectric film increases. The increased thickness does not change the reflectance minimum. In case of absorbing dielectric film, the resonance angle also increases in a linear fashion with the thickness of the dielectric film. A greater reflectance minimum with less obvious resonance angle is observed as the absorption increases. Small number of bound molecules cannot induce significant thickness and/or refractive index variation that can be detected by SPR technique. However, a small absorption of fluorophore-containing molecules undetectable by SPR technique can be recognized by the highly sensitive SPFS technique. Although the distance-dependent fluorescence quenching complicates the SPFS-generated fluorescence signal, the quantitative analysis of the SPFS-fluorescence signal can be performed on well-defined absorbing dielectric film.

Acknowledgements

S. Ekgasit gratefully acknowledges supports from the Thailand Research Fund (TRF Contract Number RSA/07/2545) and the Alexander von Humboldt (AvH) Foundation.

References

- [1] H. Raether, Surface Plasmon on Smooth and Rough Surfaces and on Gratings, Springer-Verlag, Berlin, 1988.
- [2] W. Knoll, Interfaces and thin films as seen by bound electromagnetic waves, *Annu. Rev. Phys. Chem.* 49 (1998) 569–638.
- [3] J. Homola, S.S. Yee, G. Gauglitz, Surface plasmon resonance sensors: review, *Sens. Actuators B, Chem.* 54 (1999) 3–15.

- [4] Z. Salamon, H.A. Macleod, G. Tollin, Surface plasmon resonance spectroscopy as a tool for investigating the biochemical and biophysical properties of membrane protein systems. 1. Theoretical principles, *Biochim. Biophys. Acta* 1331 (1997) 117–129.
- [5] J. Homola, Present and future of surface plasmon resonance biosensors, *Anal. Bioanal. Chem.* 377 (2003) 528–539.
- [6] R.J. Green, R.A. Frazier, K.M. Shakesheff, M.C. Davies, C.J. Roberts, S.J.B. Tendler, Surface plasmon resonance analysis of dynamic biological interactions with biomaterials, *Biomaterials* 21 (2000) 1823–1835.
- [7] T. Liebermann, W. Knoll, Surface-plasmon field-enhanced fluorescence spectroscopy, *Colloids Surf. A* 171 (2000) 115–130.
- [8] T. Neumann, M.L. Johansson, D. Kambhampati, W. Knoll, Surface-plasmon fluorescence spectroscopy, *Adv. Funct. Mater.* 12 (2002) 575–586.
- [9] T. Liebermann, W. Knoll, Parallel multispot detection of target hybridization to surface-bound probe oligonucleotides of different base mismatch by surface-plasmon field-enhanced fluorescence microscopy, *Langmuir* 19 (2003) 1567–1572.
- [10] J.W. Attridge, P.B. Daniels, J.K. Deacon, G.A. Robinson, G.P. Davidson, Sensitivity enhancement of optical immunosensors by the use of a surface-plasmon resonance fluoroimmunoassay, *Biosens. Bioelectron.* 6 (1991) 201–214.
- [11] R. Roy, J. Kim, J.T. Kellis, A.J. Poulouse Jr., C.R. Robertson, A.P. Gast, Surface plasmon resonance/surface plasmon enhanced fluorescence: an optical technique for the detection of multicomponent macromolecular adsorption at the solid/liquid interface, *Langmuir* 18 (2002) 6319–6323.
- [12] F. Yu, D.F. Yao, W. Knoll, Surface plasmon field-enhanced fluorescence spectroscopy studies of the interaction between an antibody and its surface-coupled antigen, *Anal. Chem.* 75 (2003) 2610–2617.
- [13] W.L. Barnes, Fluorescence near interfaces: the role of photonic mode density, *J. Mod. Opt.* 45 (1998) 661–699.
- [14] A. Wokaun, H.P. Lutz, A.P. King, U.P. Wild, R.R. Ernst, Energy-transfer in surface enhanced luminescence, *J. Chem. Phys.* 79 (1983) 509–514.
- [15] J.R. Lakowicz, Radiative decay engineering: biophysical and biomedical applications, *Anal. Biochem.* 298 (2001) 1–24.
- [16] I. Pockrand, A. Brillante, D. Möbius, Nonradiative decay of excited molecules near a metal-surface, *Chem. Phys. Lett.* 69 (1980) 499–504.
- [17] P. Wu, L. Brand, Resonance energy-transfer—methods and applications, *Anal. Biochem.* 218 (1994) 1–13.
- [18] M. Daffertshofer, H. Port, H.C. Wolf, Fluorescence quenching of ultrathin anthracene films by dielectric and metallic substrates, *Chem. Phys.* 200 (1995) 225–233.
- [19] N.J. Harrick, *Internal Reflection Spectroscopy*, Harrick Scientific Corporation, New York, 1987.
- [20] S. Ekgasit, C. Thammacharoen, W. Knoll, Surface plasmon resonance spectroscopy based on evanescent field treatment, *Anal. Chem.* 76 (2004) 561–568.
- [21] S. Ekgasit, C. Thammacharoen, F. Yu, W. Knoll, Evanescent field in surface plasmon resonance and surface-plasmon field-enhanced fluorescence spectroscopies, *Anal. Chem.* 76 (2004) 2210–2219.
- [22] W.N. Hansen, Electric fields produced by propagation of plane coherent electromagnetic radiation in a stratified medium, *J. Opt. Soc. Am.* 58 (1968) 380–390.
- [23] B. Valeur, *Molecular Fluorescence Principles and Applications*, Wiley/VCH, Weinheim, 2002.
- [24] J.R. Lakowicz, *Principles of Fluorescence Spectroscopy*, 2nd ed., Kluwer Academic/Plenum Publishers, New York, 1999.
- [25] R.J. Green, J. Davies, M.C. Davies, C.J. Roberts, S.J.B. Tendler, Surface plasmon resonance for real time in situ analysis of protein adsorption to polymer surface, *Biomaterials* 18 (1997) 405–413.
- [26] V. Buschmann, K.D. Weston, M. Sauer, Spectroscopic study and evaluation of red-absorbing fluorescent dyes, *Bioconjugate Chem.* 14 (2003) 195–204.
- [27] G.P. Anderson, N.L. Nerurkar, Improved fluoroimmunoassays using the dye Alexa Fluor 647 with the RAPTOR, a fiber optic biosensor, *J. Immunol. Meth.* 271 (2002) 17–24.

Biographies

Sanong Ekgasit received a BS degree in chemistry (1989) and a MS degree in polymer technology (1992) from Chulalongkorn University, Thailand, and a PhD degree in polymer science and engineering (1996) from Case Western Reserve University, USA. He has been with Department of Chemistry, Faculty of Science, Chulalongkorn University since 1998. In 2003–2004, he was an Alexander von Humboldt Research Fellow at the Max-Planck-Institut für Polymerforschung, Mainz, Germany. His research interests include Fourier transform infrared spectroscopy, surface plasmon resonance spectroscopy, and their applications.

Fang Yu received BS (1997) and MS degrees (2000) in biomedical engineering from Southeast University, Nanjing, China, and a PhD degree (2004) in biophysics from the Max-Planck-Institut für Polymerforschung (MPI-P), Mainz, Germany. Currently, he is a postdoctoral research fellow at MPI-P. His research interests are surface plasmon resonance spectroscopy, surface-plasmon field-enhanced fluorescence spectroscopy and their applications.

Wolfgang Knoll joined the Max-Planck-Institut für Polymerforschung (MPI-P) after completing his habilitation in 1986. He was appointed the director of the MPI-P in 1993. In 1991–1999, he accepted the position of head of Laboratory for Exotic Nanomaterials of the Frontier Research Program, hosted by the Institute of Physical and Chemical Research (RIKEN) in Wako, Japan. Currently, he is a Tamasek professor at the National University of Singapore, hold a professorship at the University of Florida, Gainesville, FL, USA, an adjunct professorship at Hanyang University in Seoul, Korea, and is consulting professor at Stanford University, CA, USA. His current research interests include aspects of the structure–property relationships of polymeric/organic system, with a strong emphasize on optical techniques to elucidate the structure and functional properties of supramolecular assemblies and nanomaterials.